

# Arctic System Reanalysis improvements in topographically forced winds near Greenland

G. W. K. Moore,<sup>a\*</sup> David H. Bromwich,<sup>b,c</sup> Aaron B. Wilson,<sup>b</sup> Ian Renfrew<sup>d</sup> and Lesheng Bai<sup>b</sup>

<sup>a</sup>*Department of Physics, University of Toronto, Canada*

<sup>b</sup>*Polar Meteorology Group, Byrd Polar and Climate Research Center, Ohio State University, Columbus, OH, USA*

<sup>c</sup>*Department of Geography, Ohio State University, Columbus, OH, USA*

<sup>d</sup>*School of Environmental Sciences, University of East Anglia, Norwich, UK*

\*Correspondence to: G. W. K. Moore, Department of Physics, 60 St. George Street, Toronto, Ontario, Canada, M5S 1A7.  
E-mail: gwk.moore@utoronto.ca

Southern Greenland is home to a number of weather systems characterized by high speed low-level winds that are the result of topographic flow distortion. These systems include tip jets, barrier winds and katabatic flows. Global atmospheric reanalyses have proven to be important tools in furthering our understanding of these systems and their role in the climate system. However, there is evidence that their mesoscale structure may be poorly resolved in these global products. Here output from the regional Arctic System Reanalysis (ASRv1–30 km and ASRv2–15 km grid resolutions) are compared to the global ERA-Interim Reanalysis (ERA-I–80 km grid resolution), focusing on their ability to represent winds in the vicinity of southern Greenland. Comparisons are made to observations from surface and upper-air stations, as well as from research aircraft flights during the Greenland Flow Distortion Experiment (GF Dex). The ERA-I reanalysis has a tendency to underestimate high wind speeds and overestimate low wind speeds, which is reduced in ASRv1 and nearly eliminated in ASRv2. In addition, there is generally a systematic reduction in the root-mean-square error between the observed and the reanalysis wind speeds from ERA-I to ASRv1 to ASRv2, the exception being low-level marine winds where the correspondence is similar in all reanalyses. Case-studies reveal that mesoscale spatial features of the wind field are better captured in ASRv2 as compared to the ERA-I or ASRv1. These results confirm that a horizontal grid size on the order of 15 km is needed to characterize the impact that Greenland's topography has on the regional wind field and climate. However even at this resolution, there are still features of the wind field that are under-resolved.

**Key Words:** Greenland; tip jets; flow distortion; reanalyses; barrier winds; katabatic winds

*Received 17 December 2015; Revised 18 February 2016; Accepted 19 March 2016; Published online in Wiley Online Library  
19 May 2016*

## 1. Introduction

### 1.1. Southern Greenland wind regimes

The seas surrounding southern Greenland (Figure 1) are the windiest areas of the world ocean (Sampe and Xie, 2007). The gale-force winds that occur in this region can be broadly classified as westerly or easterly tip jets (Doyle and Shapiro, 1999; Moore, 2003), northeasterly barrier winds (Moore and Renfrew, 2005), or northwesterly katabatic winds (Rasmussen, 1989). The dynamics behind these weather systems share a common factor, flow distortion resulting from the interaction of extratropical cyclones with the high and steep topography of Greenland (Moore, 2003; Moore and Renfrew, 2005; Outten *et al.*, 2009; Harden *et al.*, 2011; Oltmanns *et al.*, 2014).

In addition to their role in regional weather (Rasmussen, 1989; Renfrew *et al.*, 2008; Oltmanns *et al.*, 2014), these systems

are also important, for a variety of reasons, in the local and global climate. For example, the high winds associated with these systems have been argued to play a role in soil erosion in southern Greenland as well as contributing to the sourcing of atmospheric dust across the region (Silva-Sánchez *et al.*, 2015), a process that may contribute to the darkening of and subsequent acceleration of mass loss from the Greenland Ice Sheet (GIS) (Dumont *et al.*, 2014). High wind speeds associated with westerly tip jets have also been shown to contribute to the large losses of ocean buoyancy that drives oceanic convection in the Irminger Sea, a process that is an important component of the Atlantic Meridional Overturning Circulation (Pickart *et al.*, 2003; Våge *et al.*, 2008) as well as contributing to the oceanic sequestration of anthropogenic carbon (Sabine *et al.*, 2004).

Barrier winds have been argued to be an important contributor to regional shelf–fjord interactions that act to modulate the presence of warm Atlantic water in the fjords along Greenland's

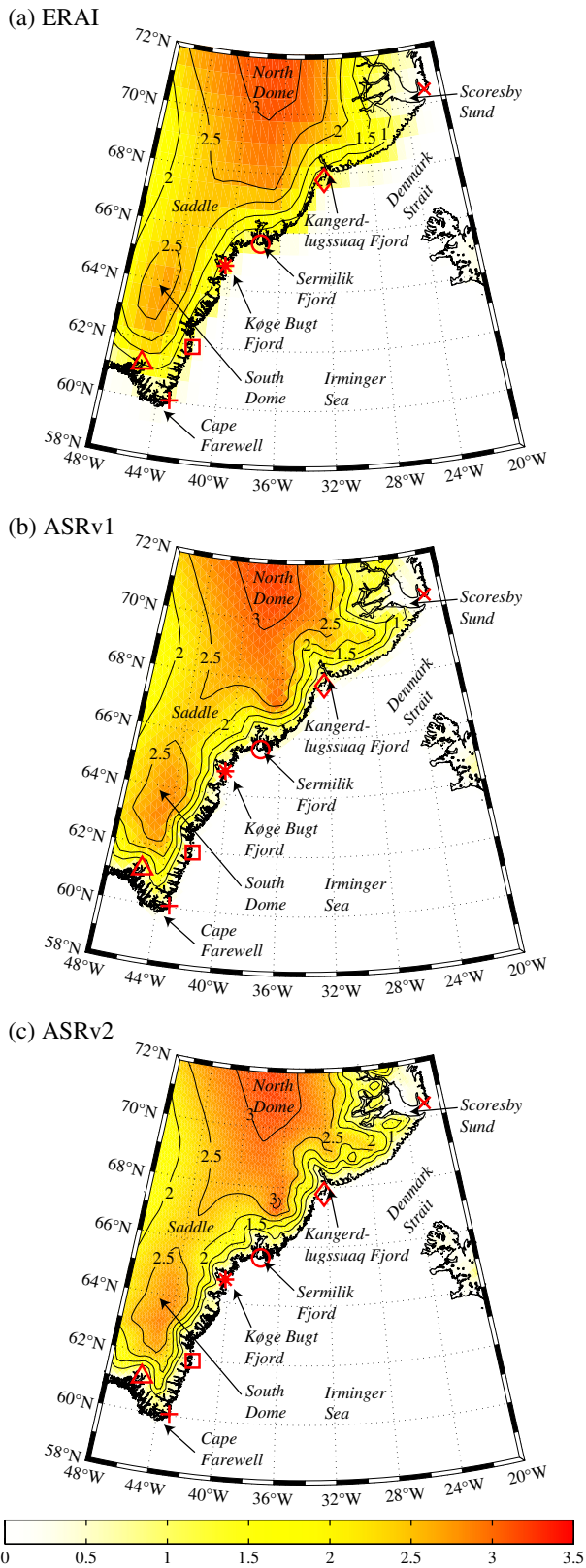


**Figure 1.** The topography (km) of southeast Greenland as represented in the: (a) ERA-I, (b) ASRv1 and (c) ASRv2. Place names of interest are shown. The ‘x’, ‘◊’, ‘o’, ‘\*’, ‘□’, and ‘+’ symbols indicate the locations of the DMI stations (from north to south) 04339, 04351, 04360, 04373, 04382 and 04390 respectively. The ‘x’, ‘o’ and ‘Δ’ symbols indicate the locations of the Ittoqqortoormiit, Tasiilaq and Narsarsuaq radiosonde sites.

southeast coast (Harden *et al.*, 2014; Straneo and Cenedese, 2015), a process that has been proposed to play a role in the retreat of the region’s marine-terminating glaciers (Howat *et al.*, 2011). These winds also play an important role in oceanic mixed-layer development, currents and shelf-break volume fluxes along the Denmark Strait (Haine *et al.*, 2009; Magaldi and Haine, 2015).

The strong outflow associated with katabatic winds can result in the loss of the ice mélange, the mixture of icebergs and sea ice that acts to inhibit calving, from the region’s marine-terminating glaciers thereby contributing to loss of mass from the GIS (Straneo and Heimbach, 2013; Oltmanns *et al.*, 2014). These winds can also advect sea ice away from the coast leading to the formation of biologically important coastal polynyas as well as leading to large losses of buoyancy in adjoining oceanic regions (Oltmanns *et al.*, 2014).

All of these weather systems are mesoscale in nature with horizontal length-scales on the order of 500 km or less (Heinemann and Klein, 2002; Moore and Renfrew, 2005; Petersen *et al.*, 2009; Renfrew *et al.*, 2009a). More generally, the complex topography of the region (Figure 1) results in small-scale variability in the surface wind field. For example, in the vicinity of Sermilik Fjord, there are two automatic weather stations that are only 16 km apart for which the correlation between the wind speeds during the winter is only 0.4 (Moore *et al.*, 2015); while observations made in the 1930s by British and Norwegian expeditions to the Kangerdlugssuaq Fjord found katabatic winds with strong lateral gradients in wind speed that were assumed to be the result of topographic sheltering (Manley, 1938).

## 1.2. The Greenland Flow Distortion Experiment and modelling flow distortion

Given the data-sparse nature of the Greenland region and the importance of topographically forced flow on the regional weather and global climate, a field campaign known as the Greenland Flow Distortion Experiment (GFDEx) was held in late February and early March 2007 to investigate this phenomenon (Renfrew *et al.*, 2008). The primary asset was a BAE 146 instrumented research aircraft that was stationed at Keflavik, Iceland during the experiment (Renfrew *et al.*, 2008). Enhanced radiosonde launches during periods of interest were also made from sites in the region, including three locations in southeast Greenland (Figure 1).

Case-studies of easterly tip jet and barrier wind events observed during GFDEx found that the limited-area version of the Met Office Unified Model operational in 2007 (version 6.1) with a horizontal resolution of 12 km was able to satisfactorily represent the structure and evolution of these weather systems, including the low-level characteristics of the observed regions of high wind speed (Outten *et al.*, 2009; Petersen *et al.*, 2009). A detailed comparison of the low-level data collected during GFDEx with operational analyses, reanalyses, both regional and global, as well as hindcasts indicated that a horizontal resolution below  $\sim 25$  km was required to adequately represent the observed spatial variability of the low-level wind field (Renfrew *et al.*, 2009b). However, such a resolution was a necessary but not sufficient condition as specifics of the atmospheric boundary layer and surface flux parametrizations used also had a significant impact on the fidelity of the representation of the surface wind field (Renfrew *et al.*, 2009b).

DuVivier and Cassano (2013) used the Weather Research and Forecasting (WRF) limited-area forecast model (Skamarock *et al.*, 2008) to investigate the tip jet and barrier wind events observed during GFDEx. For each case, the model was run at horizontal resolutions of 10, 25, 50 and 100 km and the results compared against the corresponding observed low-level and dropsonde data. This approach has the advantage of controlling for the specifics of the model’s parametrizations identified as an issue by Renfrew *et al.* (2009b). In general, the 10 km model runs were better able to capture the maxima in the observed low-level wind speeds; for example the 25 km runs underestimated the maximum low-level wind speed during the easterly tip jet event by 5–11% as compared to the 10 km model (DuVivier and Cassano, 2013). For the barrier wind event, the root-mean-square error between the observed and model wind speeds for the 10 and 25 km model runs were both  $\sim 1.5 \text{ m s}^{-1}$ , while that for the 50 km model run was  $\sim 2.6 \text{ m s}^{-1}$  suggesting that, in agreement with Renfrew *et al.*

Table 1. Specifics of the sites along the southeast coast of Greenland where surface and upper-air observations are collected during the GFDex period.

Site	ID	Vicinity	Data	Latitude	Longitude	Elevation (m)
Ittoqqortoormiit	04339	Scoresby Sund	Surface, Upper-Air	70.48°N	21.95°W	65
Aputiteeq	04351	Kangerdlugssuaq Fjord	None	67.78°N	32.30°W	13
Tasiilaq	04360	Sermilik Fjord	Surface, Upper-Air	65.60°N	37.63°W	36
Ikermiit	04373	Køge Bugt Fjord	Surface	64.78°N	40.30°W	85
Ikermiarsuk	04382	North of Cape Farewell	Surface	61.93°N	42.07°W	39
Ikerassuaq	04390	Cape Farewell	Surface	60.03°N	43.12°W	88
Narsarsuaq	04270	Cape Farewell	Upper-Air	61.15°N	45.43°W	65

Please refer to Figure 1 for the locations of these sites.

(2009b), a resolution below  $\sim 20\text{--}25$  km is needed to resolve the mesoscale variability of tip jets and barrier wind events in the vicinity of southeast Greenland.

It is clear that representations of the wind field with grid spacing sufficient to resolve the mesoscale nature of these weather systems is needed if one is to fully characterize their structure and role in the climate system (Hamilton, 2008). For example, Jung *et al.* (2014) showed that when an ocean model was forced by atmospheric fields that retain variability on the mesoscale, the strength of wind-driven gyres in the North Atlantic as well as the Atlantic Meridional Overturning Circulation was increased by 5–10% as compared to that when forced by synoptic-scale atmospheric variability alone.

In discussions of the ability of a model to capture mesoscale variability, one must distinguish between its horizontal grid resolution and the horizontal scale at which it can represent features of the atmospheric flow (Skamarock, 2004). One widely used diagnostic is to evaluate the power spectrum of the low-level kinetic energy and identify the length-scale at which the slope of the spectrum deviates from theoretical or observed spectra, with this length-scale indicating the ‘effective resolution’ (Skamarock, 2004). Typically this divergence occurs at a length-scale that is 5–7 times the horizontal resolution (Skamarock, 2004; Condron and Renfrew, 2013; Moore *et al.*, 2015), with some variation depending on model configuration. Using this metric, the effective resolution of ERA-Interim, the current global reanalysis product from the European Centre for Medium-range Weather Forecasts (ECMWF) which has a horizontal grid size of  $\sim 80$  km (Dee *et al.*, 2011), is only  $\sim 400$  km, implying that this global reanalysis product will under-resolve the mesoscale (typically 100–500 km scale) features discussed above. So although ERA-I has proven important in characterizing flows around Greenland (Harden *et al.*, 2011; Moore, 2012; Oltmanns *et al.*, 2014), it is clear that the mesoscale characteristics of these weather systems will be under-resolved by such global products.

### 1.3. Arctic System Reanalysis

The need for a high-resolution representation of the structure and variability of the Arctic troposphere is not of course limited to southeast Greenland and it was for this reason that the Arctic System Reanalysis (ASR), a regional reanalysis of the Arctic region, was initiated (Bromwich *et al.*, 2016). The ASR uses a version of WRF adapted for use in polar regions (Hines *et al.*, 2015). At present, two versions of the ASR exist, a 30 km grid size version known as ASRv1 and a 15 km grid size version

known as ASRv2, with effective horizontal resolutions of  $\sim 200$  and  $\sim 100$  km respectively. The ASR has  $\sim 26$  levels below 1 km as compared to the  $\sim 10$  levels in the ERA-I. This increased vertical resolution should result in an improved representation of boundary processes in the ASR.

During 2007, it was found that the ASRv1 and ERA-I had similar annual mean biases in surface and 500 hPa fields, with the ASRv1 generally having smaller root-mean-square errors and higher correlations (Bromwich *et al.*, 2016). In agreement with the above, Moore *et al.* (2015) found that the higher-resolution ASRv1 product was able to resolve mesoscale features of wind events in southeast Greenland better than the ERA-I. However, somewhat paradoxically, ERA-I had a lower root-mean-square error in the 10 m wind speed at the Tasiilaq station, situated outside of the Sermilik Fjord (Figure 1). This was attributed to the inability of the ERA-I to represent the downslope acceleration associated with mountain waves triggered over the steep topography to the north of the site during barrier wind events (Harden and Renfrew, 2012). The ASRv1 was able to represent this process, but not the sheltering of the site from the winds by the complex local topography leading to higher wind speeds at Tasiilaq as compared to the ERA-I and the observations.

In this article, we will merge the aforementioned research strands that have previously studied either the offshore structure of these topographically forced winds using the GFDex dataset (Outten *et al.*, 2009; Petersen and Renfrew, 2009; Petersen *et al.*, 2009; Renfrew *et al.*, 2009b; DuVivier and Cassano, 2013) or their onshore expression using observations from Greenland (Oltmanns *et al.*, 2014; Moore *et al.*, 2015). To account for the documented need for high horizontal resolution, while controlling for biases introduced by model parametrizations, we will compare and contrast the ability of the ERA-I to represent these weather systems with the ASRv1 and ASRv2.

## 2. Data

*In situ* observations from Greenland are generally limited to coastal sites maintained by the Danish Meteorological Institute (DMI). Hourly data are available from six surface stations along the southeast coast of Greenland (Figure 1 and Table 1). In addition, there are three upper-air sites in the region (Figure 1 and Table 1) where data is available on a twice-daily basis (0000 UTC and 1200 UTC). For specific cases during GFDex, additional upper-air data are available at 0600 UTC and 1800 UTC (Renfrew *et al.*, 2008).

Table 2. Specifics of the GFDex research flights considered in this article.

Flight	Date	Science aim	Area of operation	Take-off UTC	Landing UTC	Dropsondes
B268	21 February	Easterly tip jet	Cape Farewell	1048	1627	12
B271	25 February	Polar low interacting with Greenland	Iceland Sea	1035	1625	16
B274	2 March	Barrier winds	Denmark Strait	1107	1455	9
B276	5 March	Barrier winds	Denmark Strait	1120	1706	8
B277	6 March	Barrier winds	Denmark Strait	1027	1600	17
B278	9 March	Barrier winds and air-sea interaction	Denmark Strait	1031	1511	6

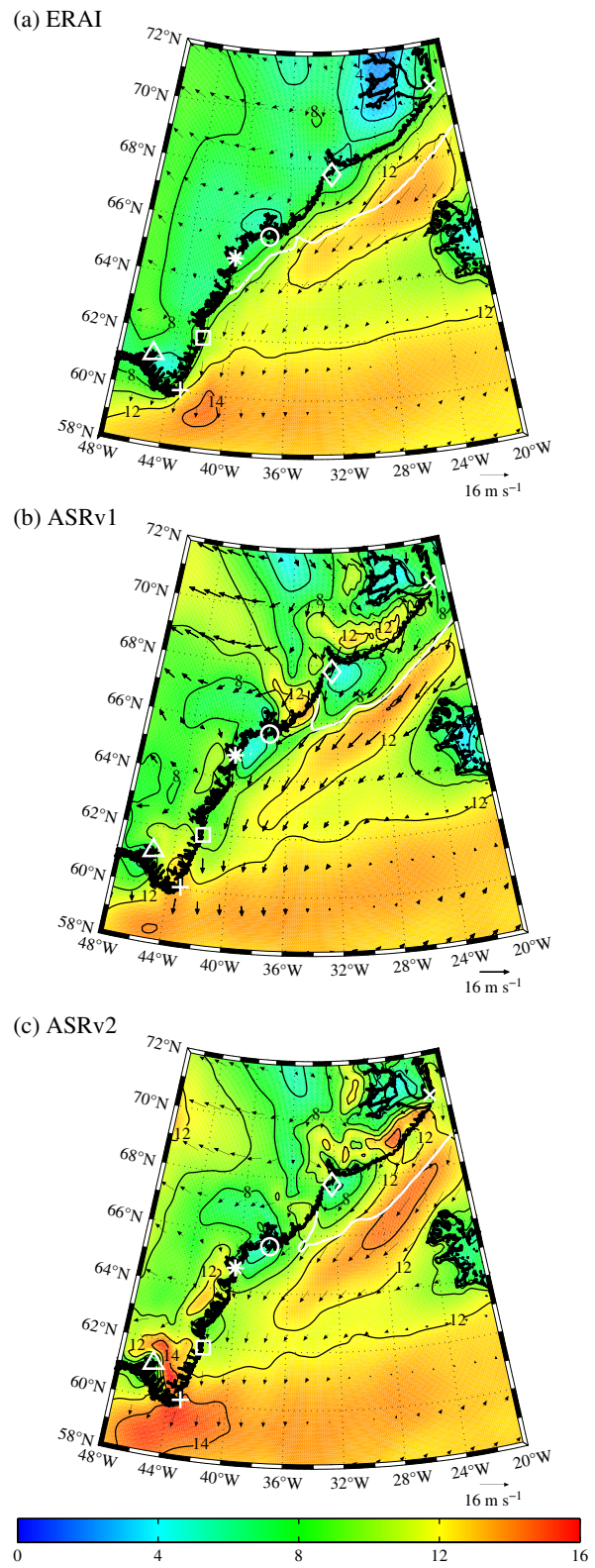
Six of the 12 research flights during GFDex collected data on the low-level wind field in the vicinity of southeast Greenland. These included a flight (B268) into an easterly tip jet (Renfrew *et al.*, 2009a), four flights (B274, B276, B277 and B278) into an evolving barrier wind event (Petersen *et al.*, 2009) and one flight (B271) into a polar low over the Iceland Sea (Renfrew *et al.*, 2008). These flights were typically organized into a high-level component, during which dropsondes were deployed to investigate the vertical structure of the system, as well as a low-level component, typically flown at heights of  $\sim 30$  m above sea-level, to sample the weather system's surface expression (Renfrew *et al.*, 2008). The low-level data that will be used in this article were quality controlled and processed into 2 min long 'runs' in which the wind speed data were adjusted to a height of 10 m using stability-dependent surface-layer similarity theory – see Petersen and Renfrew (2009b) and Renfrew *et al.* (2009b). The dropsonde data were uploaded in real time to the Global Telecommunications System and as such, were assimilated into the ERA-I and the ASR. Please refer to Table 2 for additional details on these research flights and Renfrew *et al.* (2008) for the flight tracks.

We will compare these observations with winds from ERA-I and the two ASR products during the period 15 February to 16 March 2007. The two reanalyses are the result of very different data assimilation systems and underlying numerical models with differing numerical cores, parametrizations and resolutions. For example, ERA-I is based on a global spectral model and a highly advanced four-dimensional (4D) variational data assimilation scheme; while the ASR is based on a regional grid-point model and a 3D variational data assimilation scheme that is optimized for use at high latitudes (Dee *et al.*, 2011; Bromwich *et al.*, 2016). Among the optimizations included in the ASR are the use of a land-surface scheme that includes fractional sea ice cover with variable thickness and snow cover as well as an improved representation of the albedo of snow and ice (Hines *et al.*, 2015; Bromwich *et al.*, 2016). The ERA-I data are available on a 6-hourly basis, while those from the ASR are available on a 3-hourly basis. However unless otherwise noted, the ASR data were subsampled to a 6-hourly basis.

For the comparison with the surface stations, the gridded 6-hourly ERA-I and ASR data were linearly interpolated to the location of each station. A similar approach was used for the data from the radiosonde sites. In addition, both the radiosonde and reanalysis data were interpolated to a common vertical grid with a spacing of 100 m. The aircraft data, both the low-level and dropsonde data, are available at irregular time intervals and the decision was made to interpolate the ERA-I and ASR data both temporally and spatially to the location and time that the observations were made. In this instance, the 3-hourly ASR data were used. However, a comparison with the results when the ASR data were subsampled to 6 h indicated no significant differences.

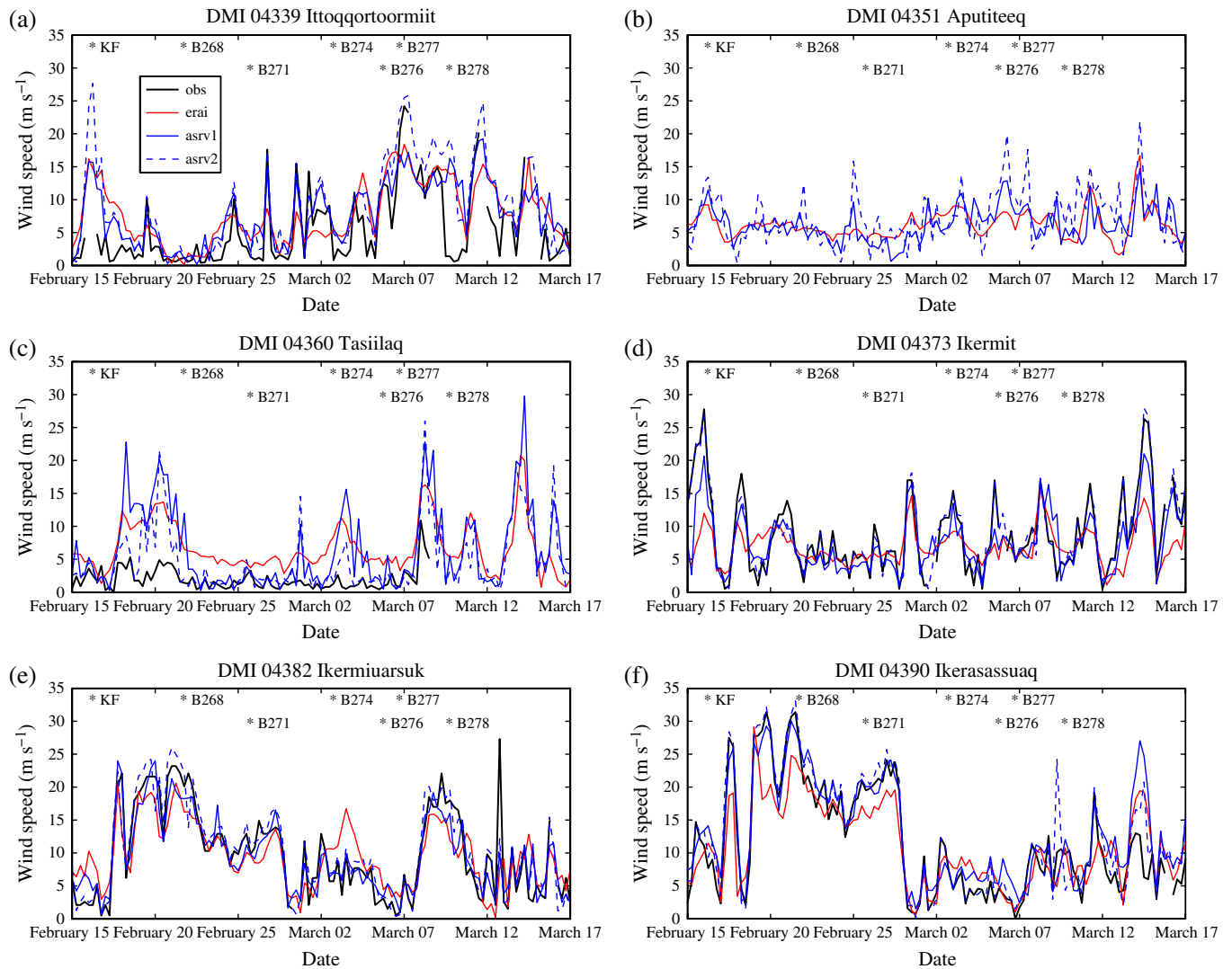
### 3. Results

Figure 1 shows the topography of the region of interest as represented in the ERA-I, ASRv1 and ASRv2. The ERA-I is able to capture the large-scale characteristics including the high topography of the South and North Domes as well as the steep coastal topography along Greenland's southeast coast. However, in comparison to the ASRv1 and ASRv2, it is clear that the coastal gradients are under-resolved as are the topographic ridges to the north of the Sermilik and Kangerdlugssuaq Fjords. In particular, the ASRv2 is able to resolve the high topography along the ridge to the north of Sermilik Fjord that contains Mount Forel, the highest point in Greenland. In addition, unlike the lower resolution topographies, the ASRv2 topography is able to resolve the catchment areas of the Køge Bugt, Sermilik and Kangerdlugssuaq Fjords that play an important role in channelling the katabatic winds that develop along these fjords (Rasmussen, 1989; Oltmanns *et al.*, 2015).



**Figure 2.** The mean 10 m wind ( $\text{vectors, } \text{m s}^{-1}$ ) and 10 m wind speed (shading and contours,  $\text{m s}^{-1}$ ) from the: (a) ERA-I, (b) ASRv1 and (c) ASRv2 for the period 15 February to 16 March 2007. The white curves are the respective 50% mean sea ice concentration contours. The 'x', '◊', 'o', '★', '□', and '+' symbols indicate the locations of the DMI stations (from north to south) 04339, 04350, 04360, 04373, 04382 and 04390 respectively. The 'x', 'o' and 'Δ' symbols indicate the locations of the Ittoqqortoormiit, Tasiilaq and Narsarsuaq radiosonde sites.

Figure 2 shows the mean 10 m wind speed and direction for the period 15 February to 16 March 2007 as represented in the ERA-I, ASRv1 and ASRv2. All three reanalyses capture the enhanced barrier flow along the Denmark Strait as well as northeasterly flow in the vicinity of Cape Farewell that result from the anomalous southeastward position of the Iceland Low during this period (Moore *et al.*, 2011). The magnitude of the wind speeds tends to



**Figure 3.** Time series of 10 m wind speed ( $\text{m s}^{-1}$ ) at the DMI sites: (a) 04339, (b) 04351, (c) 04360, (d) 04373, (e) 04382 and (f) 04390 during the period 15 February to 16 March 2007 as represented by observations (black curves) and the ERA-I (red curves), ASRv1 (blue curves) and ASRv2 (dashed blue curves). Note that there are no observations at site 04351 during this period. Also shown is the timing of the katabatic flow event observed at site 04373 (KF) as well as the low-level segments of the GFDex flights (B268, B271, B274, B276, B277 and B278).

**Table 3.** Comparison of the 10 m wind speed statistics for observations and reanalyses at DMI stations in southeast Greenland for the period 15 February to 16 March 2007.

Station no.	Root-mean-square error ( $\text{m s}^{-1}$ )			Correlation coefficient			Slope		
	ERA-I	ASRv1	ASRv2	ERA-I	ASRv1	ASRv2	ERA-I	ASRv1	ASRv2
04339	3.96	3.24	3.17	0.61	0.73	0.84	0.49	0.59	0.93
04360	4.84	4.07	2.25	0.63	0.58	0.65	1.21	2.01	1.83
04373	3.65	2.42	0.9	0.62	0.86	0.98	0.28	0.64	0.96
04382	3.41	2.08	1.67	0.76	0.9	0.93	0.52	0.75	0.93
04390	3.28	2.7	1.66	0.87	0.91	0.96	0.65	0.84	1.01
All	4.82	4.18	3.2	0.74	0.82	0.92	0.5	0.73	0.94

increase with increasing horizontal resolution, a result consistent with DuVivier and Cassano (2013). In addition, the ASRv1 and ASRv2 representations include an enhanced gradient in wind speed along the ice edge. Along the coast, the ASR representations include regions of low wind speed downwind of the Sermilik and Kangerdlugssuaq Fjords, absent from the ERA-I, that were previously proposed to be the result of sheltering (Moore *et al.*, 2015). In the vicinity of Cape Farewell, the ASR representations include a hitherto unseen onshore extension of the region of high wind speeds that is most resolved in the ASRv2. Along the southeast coast of Greenland, there is an increasing degree of fine-scale structure as one goes from the ERA-I to the ASRv2. For example, onshore of Scoresby Sund, in a region of complex topography (Figure 1), the wind field is relatively homogeneous

in the ERA-I representation but takes on a much more complex representation in the ASRv2.

Figure 3 shows time series of the 10 m wind speed at the DMI sites along with the corresponding values from the three reanalyses during the GFDex period, while Table 3 shows the relevant statistics. The northernmost station (Ittoqqortoormiit) is characterized by relatively low wind speeds during the first half of the period, while the two southernmost stations (Ikermiuarsuk and Ikerasassuaq) have much higher wind speeds. During the second half of the period this is reversed. This is consistent with the synoptic conditions experienced during the field campaign (Renfrew *et al.*, 2008). In agreement with Moore *et al.* (2015), the wind speeds at Ikermit were much higher than those at Tasiilaq. This is the result of Ikermit being exposed to katabatic flow

down the Køge Bugt Fjord, while Tasiilaq is in a more sheltered location that does not feel the influence of katabatic flow down the Sermilik Fjord.

With respect to the GFDex cases of interest, the station closest to Cape Farewell, Ikerasassuaq, clearly experienced high winds during the easterly tip jet event that was investigated during flight B268. In agreement with the results presented in Figure 2, the ERA-I significantly underestimated the wind speed at this location during this event. In contrast, the two ASR products were in much better agreement, with the ASRv2 having a slightly higher wind speed as compared to the observations and the ASRv1. The barrier wind flights (B274, B276, B277 and B278) all occurred during the period of elevated wind speeds at the northern site Ittoqqortoormiit. In particular, during flight B277, high winds were observed at this site that were associated with topographic flow distortion associated with the nearby Cape Tobin (Petersen *et al.*, 2009). As was the case for the easterly tip jet, the ERA-I underestimated the wind speed at this site during this event as compared to the observations and the ASR products.

Køge Bugt Fjord is a site where strong katabatic winds are common, and one such event is identified as KF in Figure 3. At the adjacent DMI site at Ikermit, wind speeds in excess of  $25 \text{ m s}^{-1}$  were observed; again these were underestimated in the ERA-I and to a lesser extent in the ASRv1, in contrast to the wind speed in the ASRv2 which was indistinguishable from that observed. As discussed above, the Tasiilaq site is sheltered from both the offshore barrier flow and the katabatic flow from the nearby Sermilik Fjord resulting in a relatively benign wind climate. At this site, the ERA-I tended to overestimate the wind speed as compared to the ASR products, especially during periods when the observed wind speeds were low.

Table 3 presents the mean observed and reanalysis wind speeds as well as the root-mean-square errors, correlation coefficients and slopes of the least-squares fits between the observations and reanalysis results. For each station and collectively, there is a reduction in the root-mean-square error and an increase in the correlation coefficient as well as a tendency for the regression slope to approach 1, during the transition from the ERA-I to ASRv1 to ASRv2. The only exception to a monotonic improvement in the statistics is at Tasiilaq (WMO station 04360), where the correlation and slope are worse for ASRv1 than for ERA-I. As discussed by Moore *et al.* (2015), this is the result of the complex topography in the vicinity of the station that is not fully resolved by the ASRv1. However, it is clear from Figure 3 that the ARv2 is better able to resolve the flow at this site.

Figure 4 shows scatterplots of the 10 m wind speed data from the five reporting DMI sites with the corresponding values from the three reanalyses. Consistent with Table 3, there is a reduction of the spread between the observations and reanalysis results along with an increase in the regression slope between the ERA-I and ASRv2. As a result, the pronounced bias present in the ERA-I where low wind speeds are overestimated and high wind speeds are underestimated is significantly reduced in the ASRv2. There are still instances where the ASRv2 overestimates the wind speed in low wind speed situations. It is thought that these are most likely the result of situations, like that identified by Moore *et al.* (2015), where the ASRv2 is unable to fully capture the sheltering by local topographic features.

Moving to the upper-air data, Figure 5 shows the mean observed vertical profile of wind speed, below 4 km, at the three DMI radiosonde sites, Ittoqqortoormiit, Tasiilaq and Narsarsuaq, as well as those from the three reanalyses during the GFDex period. It should be emphasized that the radiosonde data were included in the data assimilation cycles at the ECMWF and in ASR, and therefore these datasets are not independent. With respect to the northernmost site, Ittoqqortoormiit, the vertical profiles from the three reanalysis products all show a pronounced low-level jet that is absent from the observations. The reasons for this are unclear, but Petersen *et al.* (2009) found that the operational UK

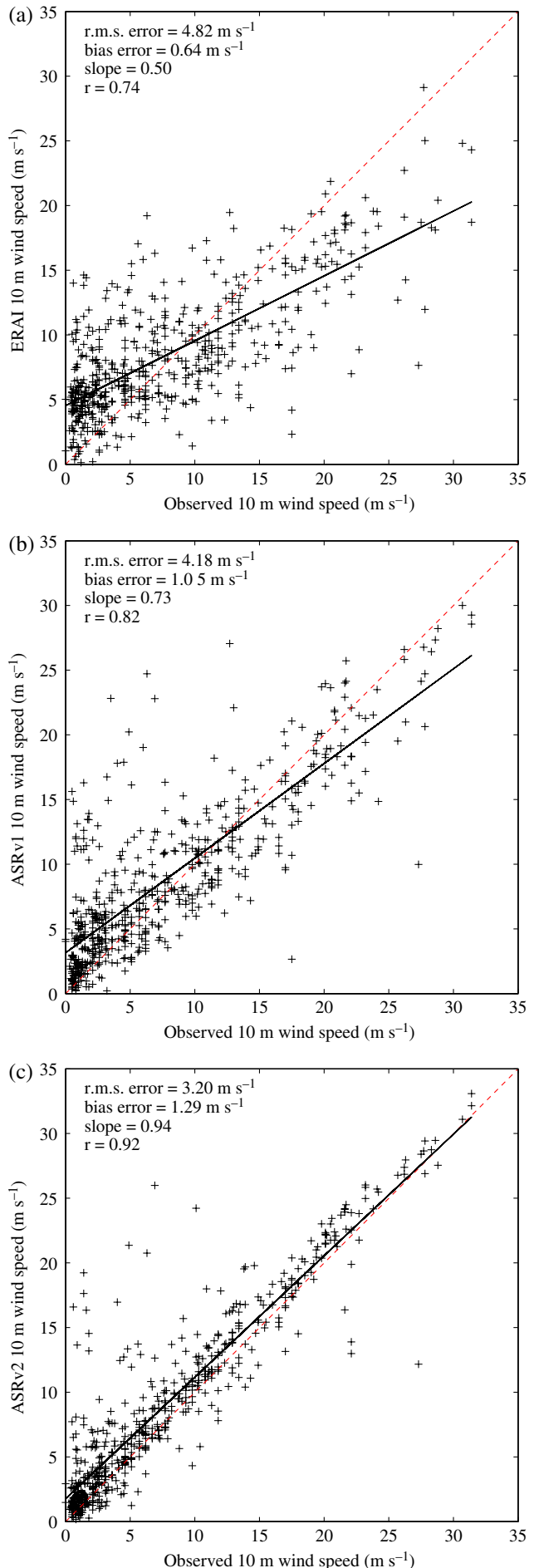
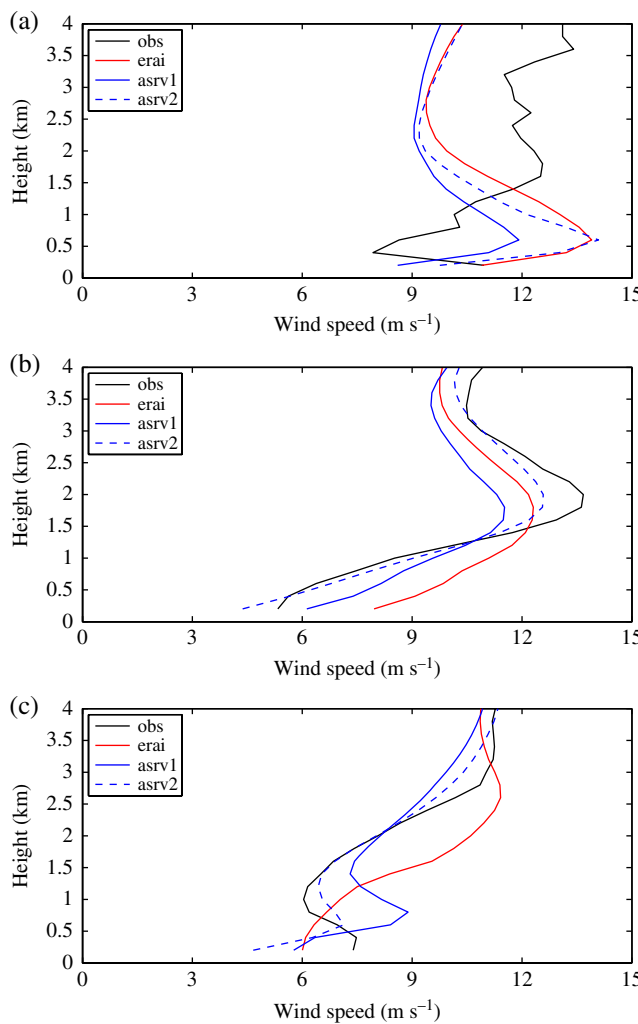


Figure 4. Scatterplot of the 10 m wind speeds ( $\text{m s}^{-1}$ ) from DMI stations and corresponding values for the period 15 February to 16 March 2007 from the: (a) ERA-I, (b) ASRv1 and (c) ASRv2. Red dashed lines are 1:1 plots. Error statistics for each fit are shown.



**Figure 5.** Comparison of the mean vertical profile of wind speed ( $\text{m s}^{-1}$ ) for the period 15 February to 16 March 2007 and corresponding profiles from the ERA-I, ASRv1 and ASRv2 for the radiosonde stations at: (a) Ittoqqortoormiit, (b) Tasiilaq and (c) Narsarsuaq.

Met Office analysis also failed to capture the observed boundary layer structure at this site during the GFDex barrier wind event. For the other two sites, the ASRv2 is better able to capture the observed mean vertical structure of the wind field as compared to the ASRv1 and ERA-I. Table 4 summarizes the error statistics of the low-level wind speed profile in the three reanalyses as compared to observations. Excluding Ittoqqortoormiit, there is a decrease in the root-mean-square error as well as an increase in the correlation coefficient and an increase in the slope of the least-squares fit lines as one transitions from the ERA-I to the ASRv2. However in comparison with Table 3, the error statistics for the wind speed profiles are less skilful than those for the 10 m wind speed.

Turning now to the comparison with the GFDex data, we present in Figure 6 scatterplots of the 10 m wind speed observed during the low-level flight legs and the corresponding reanalysis values. It should be noted that unlike the comparison with the

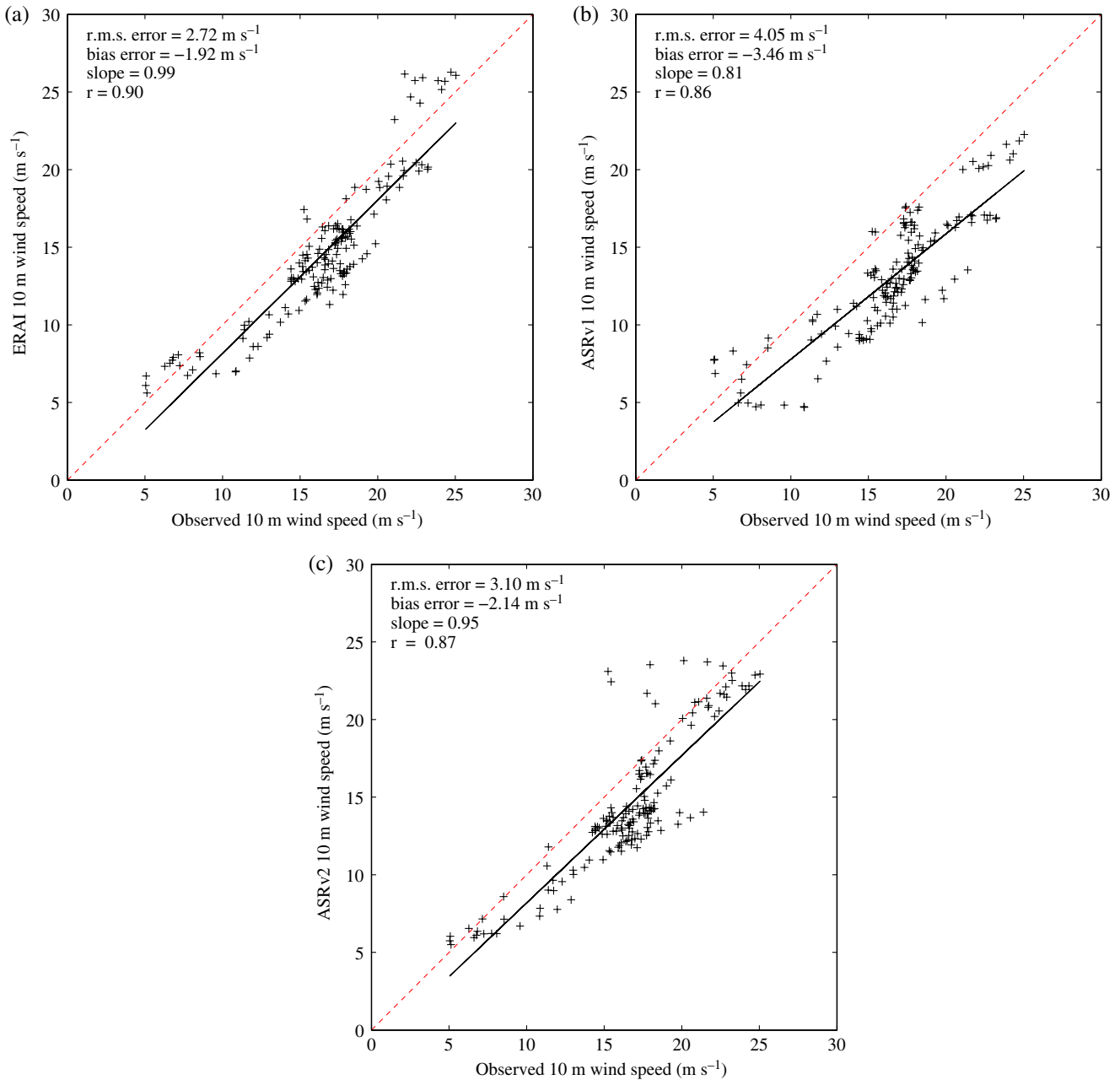
land-based observations (Figure 4), all three reanalyses had a consistent low wind speed bias across all observed wind speeds. With respect to the level of agreement, there was an improvement, i.e. a reduction in root-mean-square error and an increase in the correlation coefficient between the ASRv1 and ASRv2, suggesting that the increase in resolution allowed for an improved representation of the spatial gradients in the low-level wind field during the GFDex flights. However the error statistics between the ERA-I and ASRv2 are quite similar, implying that for this dataset, the higher grid resolution of ASRv2 has not improved the representation of the low-level wind speed. We suggest that, in agreement with Renfrew *et al.* (2009b), specifics of the underlying model's parametrizations also play a role in the representation of the low-level marine wind field associated with tip jets and barrier flow.

Table 5 provides wind speed error statistics below 4 km from the GFDex dropsonde comparison to the three reanalyses. With respect to the root-mean-square errors, there is typically a reduction in magnitude as one moves from the ERA-I to the ASRv2. The correlation coefficients and regression slopes are similar between the three reanalyses, with the ASRv2 performing better in most cases. Figure 7, which shows the scatterplots of observed and reanalysis dropsonde wind speeds during the GFDex flights, confirms the characteristics of the error statistics presented in Table 5. Although not evident from the statistics, as a result of their low numbers, Figure 7 does show that the ASRv2 is better able to represent the cases where the wind speed is in excess of  $40 \text{ m s}^{-1}$  as compared to the ERA-I and ASRv1. Comparing the wind profile comparisons from GFDex (Figure 7, Table 5) to those at Tasiilaq (Figure 5, Table 4), it is clear the reanalyses do a better job (lower root-mean-square errors and improved correlations) for the former and the improvement with resolution is smaller. Again we suggest that this is because the GFDex data are primarily marine locations, so improvements due to higher resolution are modest.

Having provided a number of more quantitative measures of the impact that resolution has on the ability of the three reanalyses to represent the observed low-level wind speed around southern Greenland, we will finish with a more qualitative comparison that is based on three events during the GFDex period. Figure 8 shows the sea-level pressure, 10 m wind and 10 m wind speed fields as represented by the three reanalyses during the easterly tip jet event sampled during flight B268 (Table 2). At this time, the parent synoptic-scale low was situated to the southeast of Cape Farewell (Renfrew *et al.*, 2009a) and as a result, the region of interest was under the influence of northeasterly flow. All three reanalyses were able to capture the synoptic-scale pressure gradient associated with this system. The ERA-I had a broad region of high pressure over eastern portions of the GIS. In the ASR products, this feature was reduced to a mesoscale region of high pressure in the vicinity of the Køge Bugt Fjord, a result in agreement with the case-study of this event (Outten *et al.*, 2009). On the eastern side of Greenland, a ridge associated with this feature couples with a trough that extends along the west coast of Greenland towards Cape Farewell to enhance the pressure gradient that is associated with high wind speeds in the core of the tip jet. In the ASR products, the presence of a mesoscale low downwind of Cape Farewell results in an enhancement of the gradient and the

**Table 4.** Comparison statistics between wind speed and corresponding values from the ERA-I, ASRv1 and ASRv2 for radiosonde stations in the vicinity of southeast Greenland during the period 15 February to 16 March 2007.

Station	Root-mean-square error ( $\text{m s}^{-1}$ )			Correlation coefficient			Slope		
	ERA-I	ASRv1	ASRv2	ERA-I	ASRv1	ASRv2	ERA-I	ASRv1	ASRv2
Ittoqqortoormiit	7.19	7.46	7.62	0.5	0.43	0.43	0.4	0.28	0.34
Tasiilaq	5.48	4.75	3.61	0.76	0.81	0.89	0.76	0.74	0.88
Narsarsuaq	4.17	4.06	2.33	0.83	0.85	0.95	0.81	0.92	0.92
All	5.70	5.58	5.00	0.70	0.71	0.77	0.65	0.63	0.71



**Figure 6.** Scatterplot of the 10 m wind speeds ( $\text{m s}^{-1}$ ) from GFDex low-level flight legs and corresponding values from the: (a) ERA-I, (b) ASRv1 and (c) ASRv2. Red dashed lines are 1:1 plots. Error statistics for each fit are shown.

Table 5. Comparison statistics between wind speeds and corresponding values from the ERA-I, ASRv1 and ASRv2 for the dropsondes from the GFDex flights.

Flight	Root-mean-square error ( $\text{m s}^{-1}$ )			Correlation coefficient			Slope		
	ERA-I	ASRv1	ASRv2	ERA-I	ASRv1	ASRv2	ERA-I	ASRv1	ASRv2
B268	3.27	3.75	3.34	0.87	0.84	0.89	0.76	0.56	0.90
B271	2.90	2.86	2.64	0.80	0.82	0.85	0.78	0.74	0.83
B274	3.12	4.27	3.33	0.90	0.81	0.89	0.77	0.68	0.79
B276	2.12	2.06	1.92	0.89	0.90	0.91	0.77	0.78	0.77
B277	4.56	3.19	2.81	0.75	0.86	0.90	0.64	0.70	0.80
B278	4.08	3.00	2.34	0.59	0.75	0.81	0.87	0.63	0.78
All	3.56	3.28	2.82	0.90	0.91	0.94	0.90	0.89	0.91

concomitant high winds in the vicinity of Cape Farewell. This feature is also present in the simulations of Outten *et al.* (2009).

One consequence of the presence of this mesoscale low in the ASR products is a region with a large horizontal pressure gradient that extends northwards from Cape Farewell towards the South Dome of the GIS (Figure 1). This gradient results in an onshore extension of the high wind speeds associated with the tip jet, a feature that is absent in the ERA-I. The gradient is stronger in the ASRv2 as are the wind speeds in the core of the jet. Indeed, there

is an approximate 25% increase in the peak 10 m wind speed associated with the tip jet in the ASRv2 as compared to the ERA-I.

Details on the vertical structure of the tip jet and its onshore extension are provided in Figure 9. Consistent with Figure 8, ERA-I does not resolve the onshore extension of the tip jet in the vicinity of Narsarsuaq. The ASRv1 tends to overestimate its magnitude, most likely as a result of errors in the placement of the mesoscale low, while the ASRv2 is in good agreement. It should be noted that the Narsarsuaq observations indicated the

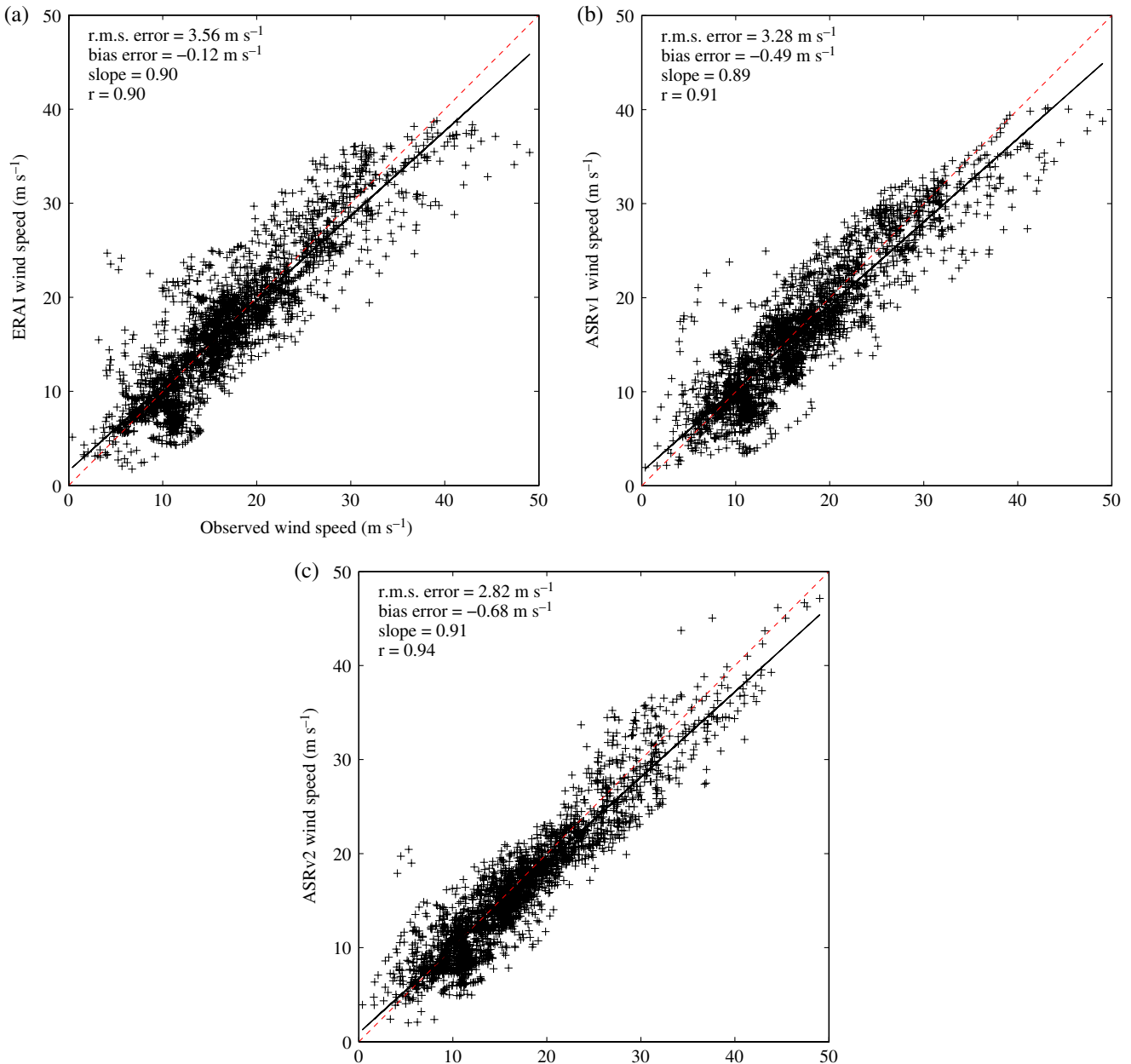


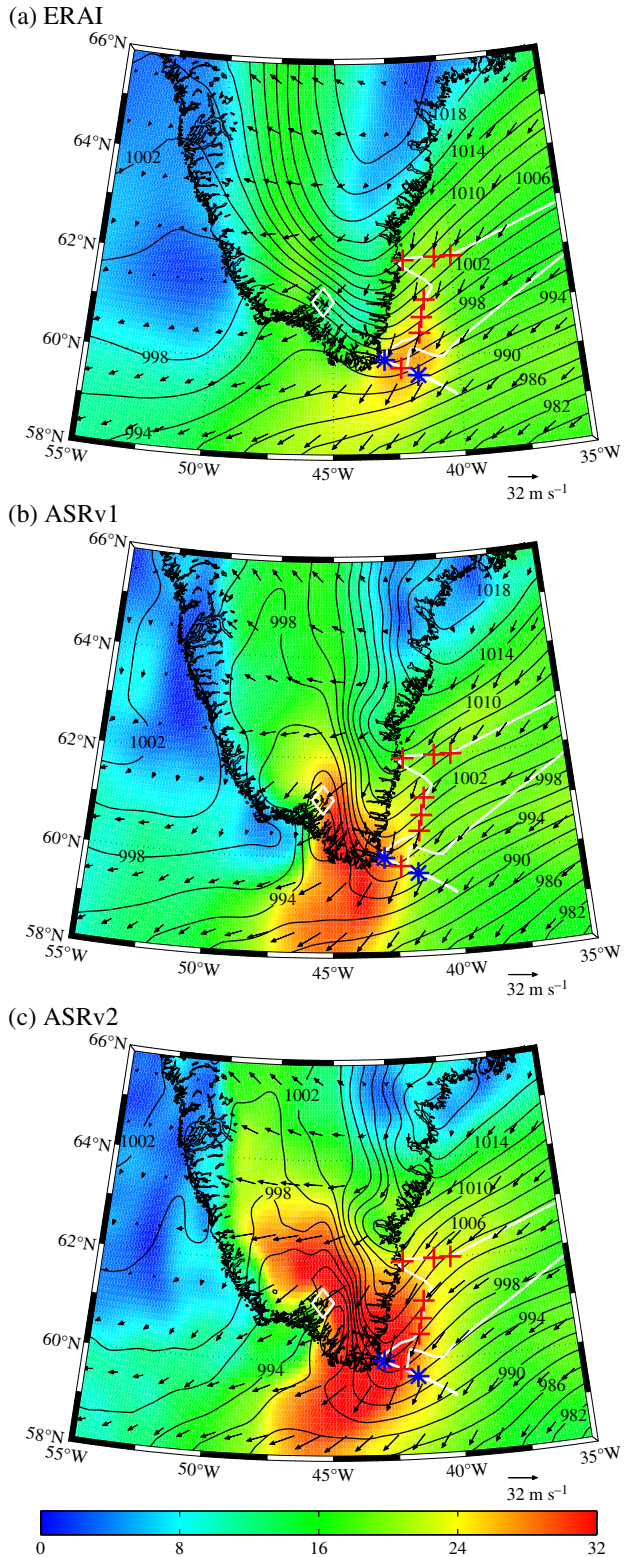
**Figure 7.** Comparison of observed dropsonde wind speeds ( $\text{m s}^{-1}$ ) from GFDex topographic flow distortion flights and corresponding values from the: (a) ERA-I, (b) ASRv1 and (c) ASRv2. Red dashed lines are 1:1 plots. Error statistics for each fit are shown.

presence of wind speed perturbations above 2 km that are most likely the result of gravity wave activity that are not captured in any of the reanalyses. The two dropsonde profiles were selected so as to provide information on the wind speed gradient on the eastern flank of the tip jet (Figure 8). Again the ERA-I and the ASRv1 are unable to capture the high wind speeds in the core of the tip jet as represented in the 1321 UTC dropsonde. In contrast, the ASRv2 does a much better job with a maximum wind speed of  $\sim 46 \text{ m s}^{-1}$  as compared to the observed maximum of  $\sim 49 \text{ m s}^{-1}$ . This is in agreement with the results of Outten *et al.* (2009). On the eastern flank of the tip jet, all of the reanalyses underestimate the highest wind speeds, with the ERA-I and ASRv2 performing best.

Figure 10 shows the sea-level pressure, 10 m wind and 10 m wind speed fields as represented by the three reanalyses during the barrier wind event sampled during flight B277 (Table 2). The aircraft data were centred  $\sim 1500$  UTC and so for this case the ERA-I data at 1200 UTC and 1800 UTC were averaged to provide data at this time. For this event, the parent low was situated off the southeast coast of Iceland, and the Denmark Strait region was under the influence of its synoptic-scale pressure gradient (Petersen *et al.*, 2009). As was the case for the tip jet event, there is a region of high pressure over Greenland

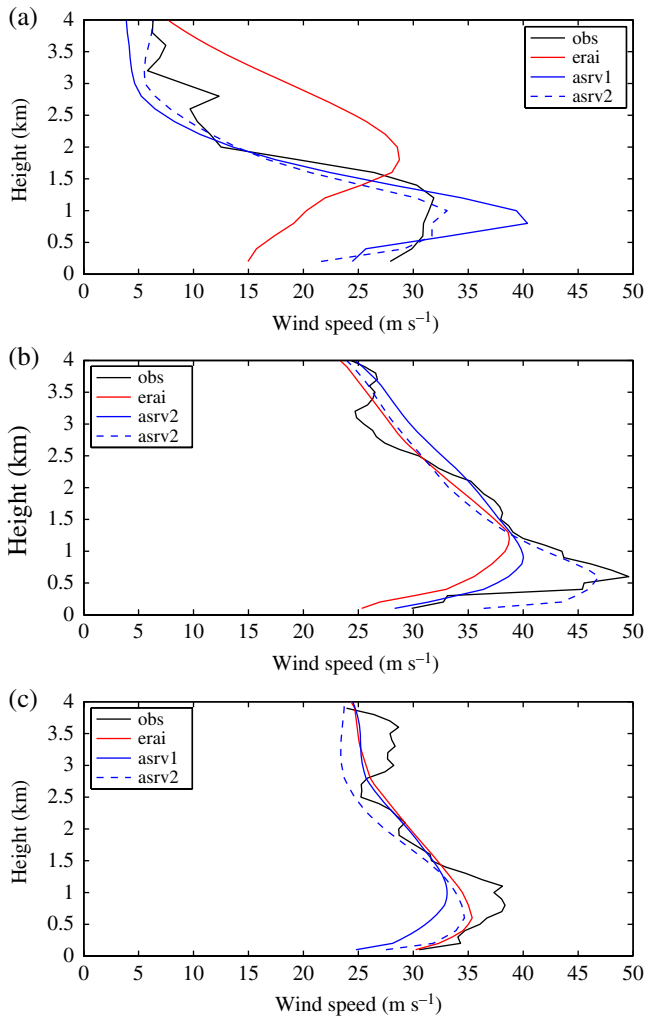
that takes on a more complex shape as one moves from the ERA-I to the ASRv2. There is also a pressure trough along the southeast coast of Greenland extending southwards from Scoresby Sund towards Kangerdlugssuaq Fjord (Figure 1) that takes on higher-order structure in the ASR products that includes the presence of a mesoscale low downwind of Kangerdlugssuaq Fjord. Again, moving from the ERA-I to the ASRv2 results in an approximate 25% increase in the maximum 10 m wind speeds in the barrier flow. The 10 m wind speed distribution over the Denmark Strait can be seen to be an interplay between the mesoscale features of sea-level pressure field and the distribution of sea ice. As a result of its ability to capture the mesoscale structure of the sea-level pressure field, the ASRv2 contains a signature of the left-hand corner jet offshore of Cape Tobin, the most easterly point along the southeast coast of Greenland (Petersen *et al.*, 2009).

Figure 11 shows wind speed profiles from the Ittoqqortoormiit radiosonde launch at 1200 UTC alongside those from two dropsondes released during flight B277. As was found to be the case for the monthly mean vertical profiles, there is a significant disagreement between the observed and reanalysis wind speed profiles at Ittoqqortoormiit. In particular, all three reanalyses contain a representation of a low-level jet that is most likely



**Figure 8.** Atmospheric circulation during the B268 GFDEX mission at 1200 UTC on 21 February 2007. The sea-level pressure (hPa, contours), 10 m wind ( $\text{m s}^{-1}$ , vectors) and 10 m wind speed ( $\text{m s}^{-1}$ , shading) as represented in the: (a) ERA-I, (b) ASRv1 and (c) ASRv2. The UK Facility for Airborne Atmospheric Measurements (FAAM) flight plan is shown as the white curve along with the locations of the dropsondes, indicated by the '+' and 'x', that were launched. The site of the Narsarsuaq radiosonde station is indicated by the '◊'. Data from the dropsondes indicated by the '\*' and the Narsarsuaq radiosonde are shown in Figure 9.

associated with the feature seen in the vicinity of Cape Tobin at this time (Figure 10). Again, there is good agreement between the ERA-I and ASRv2 with respect to the maximum wind speed. Offshore, the 1409 UTC dropsonde was situated in the entrance region of the barrier flow that was situated over the marginal ice zone. All three reanalyses were able to capture the shallow nature of the jet at this time with the ASRv2 coming closest



**Figure 9.** Vertical profile of wind speed ( $\text{m s}^{-1}$ ) on 21 February 2007 during the B268 easterly tip jet flight from: (a) the 1200 UTC Narsarsuaq radiosonde, (b) the 1321 UTC dropsonde no. 9 and (c) the 1324 UTC dropsonde no. 11 along with the corresponding wind speeds from the ERA-I, ASRv1 and ASRv2.

to the observed wind speed in the core of the jet. However all reanalyses underestimated the low-level wind speed. The 1459 UTC dropsonde was located along the onshore flank of the barrier jet close to the ice edge. For this dropsonde, all three reanalyses underestimate the maximum wind speed at this location, with the ERA-I and ASRv2 again coming close to the observed maximum. Unlike what occurred at the site of the 1409 UTC dropsonde, all three reanalyses were in good agreement with the observations with respect to the low-level wind speeds below the jet core. In addition at this location, the ERA-I, unlike the ASR products, was unable to capture the strong vertical shear above the jet core. There is also evidence of gravity wave activity in both dropsondes that is absent from all the reanalyses. Wave-like features in the clouds were observed from the research aircraft during this event.

We conclude with an example of a katabatic flow event. On 16 February 2007, the DMI station at Ikermit, offshore of the Køge Bugt Fjord (Figure 1), reported a 10 m wind speed in excess of  $25 \text{ m s}^{-1}$  (Figure 3(d)). We show in Figure 12 the sea-level pressure, 10 m wind and 10 m wind speed fields at 0000 UTC on 16 February. At this time, the parent low was situated near  $63^\circ\text{N}$ ,  $25^\circ\text{W}$ . The ASR products capture the formation of a region of high pressure along the coast to the south of the fjord as well as a region of low pressure upwind of the fjord. As a result of these mesoscale features, there is an enhanced pressure gradient in the ASR products that results in strong outflow in the vicinity of the fjord that extends a considerable distance offshore. In this instance, the maximum 10 m wind speeds in the ERA-I are  $\sim 12$  and  $\sim 32 \text{ m s}^{-1}$  in the ASRv2. Oltmanns *et al.* (2015) found a similar increase in wind speed with increasing horizontal

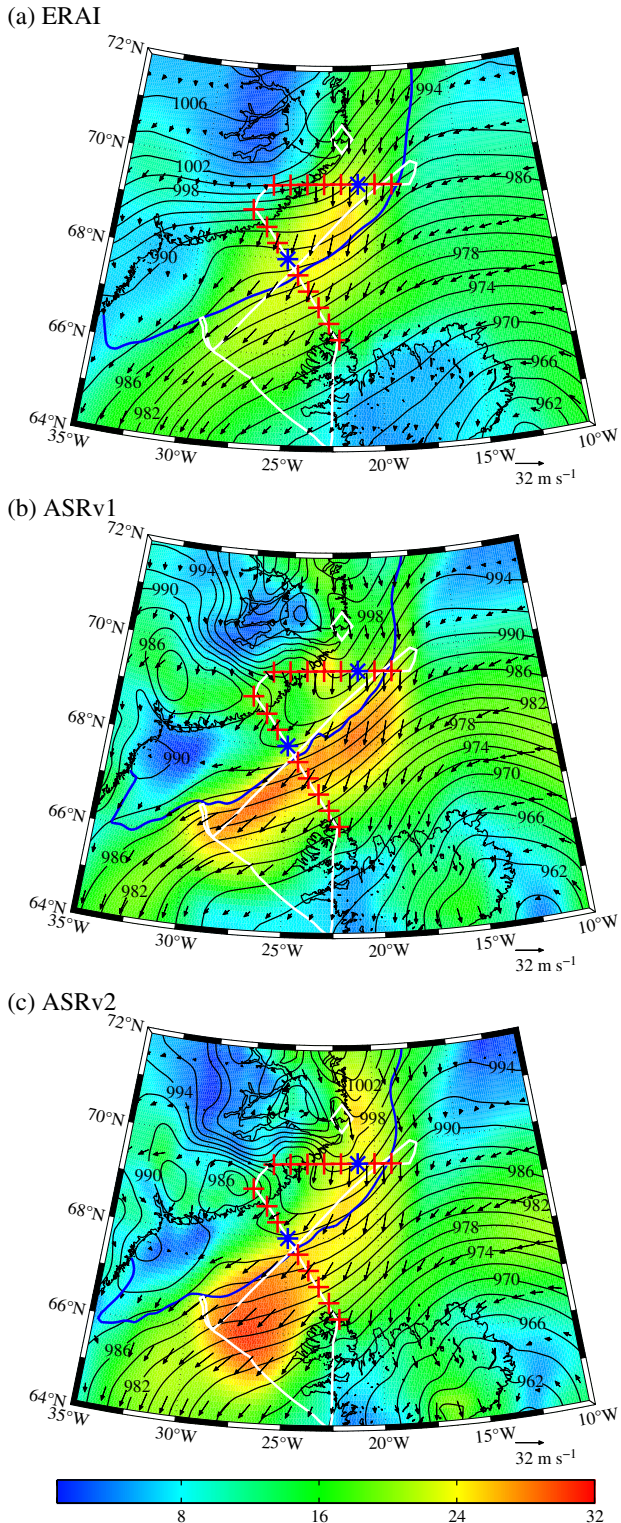


**Figure 10.** Atmospheric circulation during the B277 GFDex mission at 1500 UTC on 6 March 2007. The sea-level pressure (hPa, contours), 10 m wind ( $\text{m s}^{-1}$ , vectors) and 10 m wind speed ( $\text{m s}^{-1}$ , shading) as represented in the: (a) ERA-I, (b) ASRv1 and (c) ASRv2. The FAAM flight plan is shown as the white curve along with the locations of the dropsondes, indicated by the '+' and '\*', that were launched. The 50% sea ice concentration profile from the respective dataset is indicated by the thick blue contour. The site of the Itoqqortoormiit radiosonde station is indicated by the ' $\diamond$ '. Data from the dropsondes indicated by the '\*' and the Itoqqortoormiit radiosonde are shown in Figure 11.

resolution for a case-study of katabatic flow within the Sermilik Fjord.

#### 4. Discussion

Southern Greenland's high topography combined with its location along the primary North Atlantic storm track results

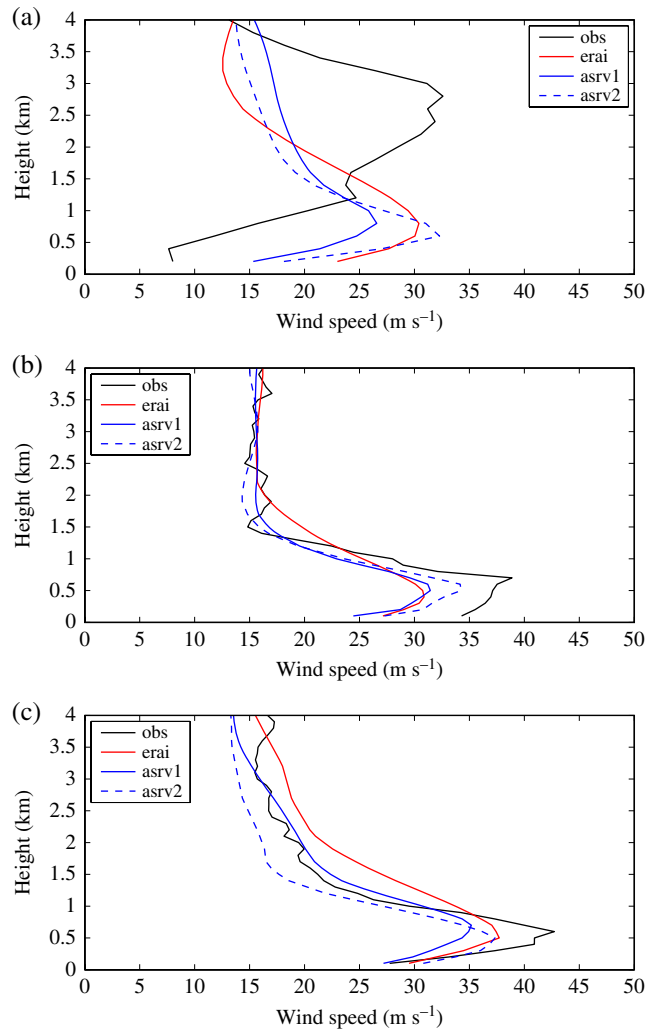


**Figure 11.** Vertical profile of wind speed ( $\text{m s}^{-1}$ ) on 6 March 2007 during the B277 barrier wind flight from: (a) the 1200 UTC Itoqqortoormiit radiosonde, (b) the 1409 UTC dropsonde no. 3 and (c) the 1459 UTC dropsonde no. 12 along with the corresponding wind speeds from the ERA-I, ASRv1 and ASRv2.

in a number of low-level high wind speed weather systems that are the result of topographic flow distortion. The systems include tip jets, barrier winds and katabatic flow that all play important roles in regional weather and global climate. Given the remote and data-sparse nature of the region along with its inhospitable weather, numerical models, including atmospheric reanalyses, have played a key role in the characterization of these systems and their impacts. These systems all have mesoscale characteristics and there is evidence that global reanalyses such as the ERA-I, while providing much information on their structure, may under-resolve these characteristics. The recent availability of high-resolution regional reanalyses of the Arctic as represented by the ASR provides a hitherto unavailable opportunity to more completely characterize these weather systems and their role in the climate system.

This study is unique in that it looks at both onshore and offshore representation of topographic flow distortion in the ERA-I and ASR using operational observations from DMI sites and GFDex observations. Previous work has identified the important role that differing model parametrizations have on the representation of these weather systems (Renfrew *et al.*, 2009b) and the inclusion of both the 30 km ASRv1 and 15 km ASRv2 products allows for a partial control of this effect.

Increasing horizontal resolution improves the representation of the onshore structure of topographically forced flow in southeast Greenland as evidenced by an elimination of low and high wind speed biases, smaller root-mean-square errors, higher correlation coefficients and regression slopes closer to 1 for both the surface winds (Table 3; Figure 4) and the upper-level winds (Table 4;

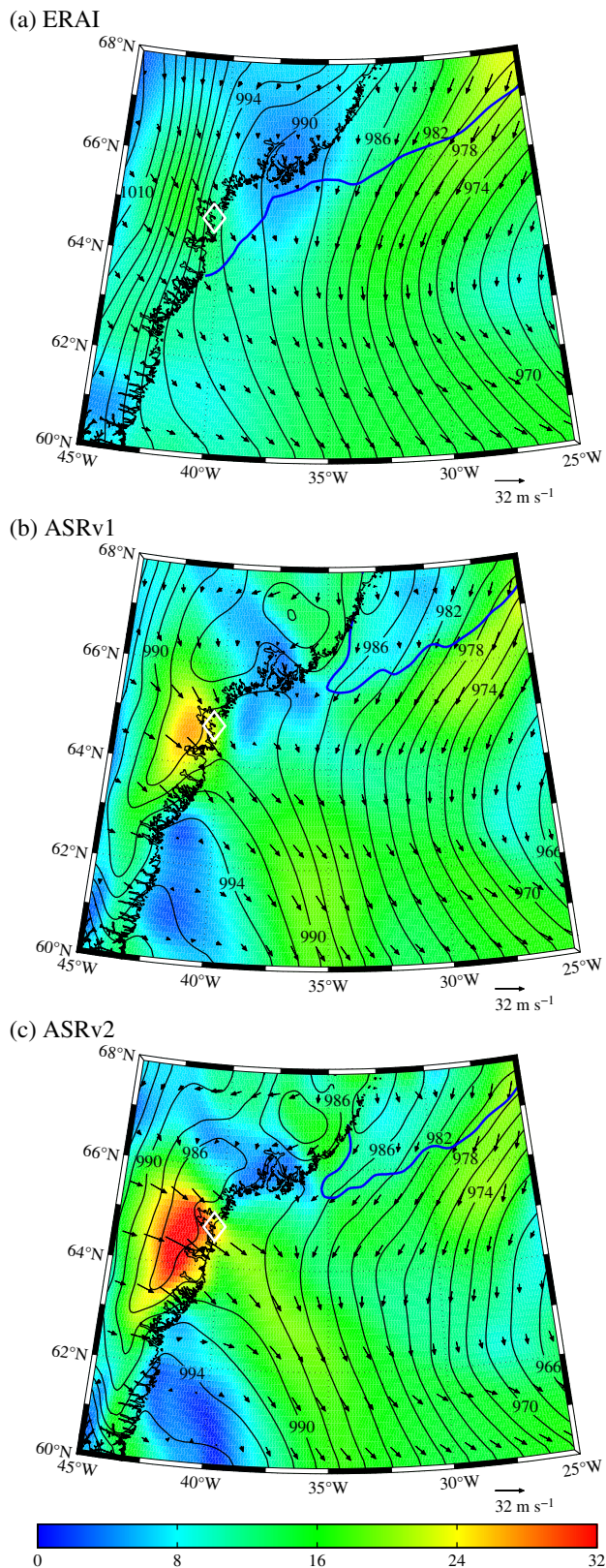


**Figure 12.** Atmospheric circulation during the Køge Bugt Fjord katabatic flow event at 0000 UTC on 16 February 2007. The sea-level pressure (hPa, contours), 10 m wind ( $\text{m s}^{-1}$ , vectors) and 10 m wind speed ( $\text{m s}^{-1}$ , shading) as represented in the: (a) ERA-I, (b) ASRv1 and (c) ASRv2. The 50% sea ice concentration profile from the respective dataset is indicated by the thick blue contour. The site of the DMI station that observed the event is indicated by the ‘◇’.

Figure 5). In contrast for the GFDex low-level flights, there was no appreciable difference between the error statistics for the ERA-I and ASR products (Figure 6). However, the GFDex dropsonde data did show a general improvement in the goodness of fit with observations between the ERA-I and the ASRv2. This suggests that increasing horizontal resolution does play a role in improving the representation of these weather systems but that

the parametrization of the marine boundary layer also plays an important role. There is also indirect evidence from the dropsonde data over the marginal ice zone (Figure 11(b)) that both the ERA-I and ASR may overestimate the surface roughness in this region.

In general, there was a 10–20% underestimation in peak wind speeds in tip jets, barrier winds and katabatic winds in the ERA-I as compared to the ASRv2. This is in agreement with previous work (DuVivier and Cassano, 2013; Moore *et al.*, 2015) and suggests that the impact of these weather systems, including the forcing of deep ocean convection, are under-resolved in the current generation of climate models that have a horizontal resolution on the order of 100 km (Kinter *et al.*, 2013). Indeed, Jung *et al.* (2014) showed a significant 5–10% increase in the strength of surface and deep ocean currents when an ocean model was forced with atmospheric fields with a horizontal resolution of 40 km as compared to that when only synoptic-scale variability was retained. This suggests further impacts on the strength of the oceanic circulations can be expected from higher-resolution representations of the forcing associated with these weather systems.

Global reanalyses with horizontal resolutions higher than that for ERA-I, such as the Climate Forecast System Reanalysis (Saha *et al.*, 2010) with a horizontal resolution of ~40 km and the JRA55 (Ebita *et al.*, 2011) with a horizontal resolution of ~50 km, were also investigated with respect to their ability to represent orographic flow near Greenland. For both of these reanalyses, no systematic improvement over the ERA-I was found, and the comparisons against observations were qualitatively similar to the ERA-I.

New features of topographic flow distortion in southeast Greenland were also identified with the ASR products. Among these is an onshore extension of the high winds associated with the easterly tip jets (Figures 8 and 9). This region of high winds that extends from the South Dome to Cape Farewell was most apparent in the ASRv2. It appears to be associated with a mesoscale low that develops in the lee of Cape Farewell. Such lows have been predicted to develop as a hydrostatic response to flow impinging on a topographic barrier (Smith, 1982). Petersen *et al.* (2009) suggested that barrier flow along Greenland's southeast coast results in the formation of a ‘corner’ jet near Cape Tobin, the promontory at the mouth of Scoresby Sund (Figure 1). The ASR reanalyses also show this jet and indicate that a horizontal resolution of 15 km is needed to fully represent it (Figure 10). The onshore 10 m wind field in the vicinity of Scoresby Sund also exhibits more complex spatial variability in the ASRv2 as compared to the ERA-I that is most likely the result of higher spatial resolution that can better represent the complex topographic and land-use gradients in this region. The Køge Bugt Fjord has been previously identified as a region where intense katabatic winds can develop (Moore *et al.*, 2015). The ASRv2 provides additional information on the structure of this flow including an increase in the 10 m wind speed and an offshore region of elevated wind speeds.

### Acknowledgements

This work was supported by the Natural Sciences and Engineering Research Council of Canada as well as the National Aeronautics and Space Administration (NASA) grant NNX12AI29G. The authors thank the Ohio Supercomputer Center (<http://www.osc.edu>) for their use of the Glenn, Oakley and Ruby Clusters in order to conduct the ASR. The authors would also like to acknowledge the participants in the Greenland Flow Distortion Experiment whose data collection activities were central to this article. This is Contribution 1543 of the Byrd Polar and Climate Research Center.

### References

- Bromwich DH, Wilson AB, Bai L-S, Moore GWK, Bauer P. 2016. A comparison of the regional Arctic System Reanalysis and the global ERA-Interim Reanalysis for the Arctic. *Q. J. R. Meteorol. Soc.* 142: 644–658.

- Condron A, Renfrew IA. 2013. The impact of polar mesoscale storms on northeast Atlantic Ocean circulation. *Nat. Geosci.* **6**: 34–37.
- Dee DP, Uppala SM, Simmons AJ, Berrisford P, Poli P, Kobayashi S, Andrae U, Balmaseda MA, Balsamo G, Bauer P, Bechtold P, Beljaars ACM, van de Berg L, Bidlot J, Bormann N, Delsol C, Dragani R, Fuentes M, Geer AJ, Haimberger L, Healy SB, Hersbach H, Hölm EV, Isaksen L, Källberg P, Köhler M, Matricardi M, McNally AP, Monge-Sanz BM, Morcrette JJ, Park B-K, Peubey C, de Rosnay P, Tavolato C, Thépaut J-N, Vitart F. 2011. The ERA-Interim reanalysis: Configuration and performance of the data assimilation system. *Q. J. R. Meteorol. Soc.* **137**: 553–597.
- Doyle JD, Shapiro MA. 1999. Flow response to large-scale topography: The Greenland tip jet. *Tellus A* **51**: 728–748.
- Dumont M, Brun E, Picard G, Michou M, Libois Q, Petit J-R, Geyer M, Morin S, Josse B. 2014. Contribution of light-absorbing impurities in snow to Greenland's darkening since 2009. *Nat. Geosci.* **7**: 509–512.
- DuVivier AK, Cassano JJ. 2013. Evaluation of WRF model resolution on simulated mesoscale winds and surface fluxes near Greenland. *Mon. Weather Rev.* **141**: 941–963.
- Ebita A, Kobayashi S, Ota Y, Moriya M, Kumabe R, Onogi K, Harada Y, Yasui S, Miyaoka K, Takahashi K, Kamahori H, Kobayashi C, Endo H, Soma M, Oikawa Y, Ishimizu T. 2011. The Japanese 55-year reanalysis: An interim report. *SOLA* **7**: 149–152.
- Haine TWN, Zhang S, Moore GWK, Renfrew IA. 2009. On the impact of high-resolution, high-frequency meteorological forcing on Denmark Strait ocean circulation. *Q. J. R. Meteorol. Soc.* **135**: 2067–2085.
- Hamilton K. 2008. Numerical resolution and modeling of the global atmospheric circulation: a review of our current understanding and outstanding issues. In *High Resolution Numerical Modelling of the Atmosphere and Ocean*, Hamilton K, Ohfuchi W. (eds.): 7–27. Springer: New York, NY.
- Harden BE, Renfrew IA. 2012. On the spatial distribution of high winds off southeast Greenland. *Geophys. Res. Lett.* **39**: L14806, doi: 10.1029/2012GL052245.
- Harden BE, Renfrew IA, Petersen GN. 2011. A climatology of wintertime barrier winds off southeast Greenland. *J. Clim.* **24**: 4701–4717.
- Harden BE, Straneo F, Sutherland DA. 2014. Moored observations of synoptic and seasonal variability in the East Greenland Coastal Current. *J. Geophys. Res. Oceans* **119**: 8838–8857, doi: 10.1002/2014JC010134.
- Heinemann G, Klein T. 2002. Modelling and observations of the katabatic flow dynamics over Greenland. *Tellus A* **54**: 542–554.
- Hines KM, Bromwich DH, Bai L, Bitz CM, Powers JG, Manning KW. 2015. Sea ice enhancements to polar WRF. *Mon. Weather Rev.* **143**: 2363–2385.
- Howat IM, Ahn Y, Joughin I, van den Broek MR, Lenaerts JTM, Smith B. 2011. Mass balance of Greenland's three largest outlet glaciers, 2000–2010. *Geophys. Res. Lett.* **38**: L12501, doi: 10.1029/2011GL047565.
- Jung T, Serrar S, Wang Q. 2014. The oceanic response to mesoscale atmospheric forcing. *Geophys. Res. Lett.* **41**: 1255–1260.
- Kinter JL III, Cash B, Achuthavarier D, Adams J, Altshuler E, Dirmeyer P, Doty B, Huang B, Jin EK, Marx L, Manganello J, Stan C, Wakefield T, Palmer TN, Hamrud M, Jung T, Miller M, Towers P, Wedi N, Satoh M, Tomita H, Kodama C, Nasuno T, Oouchi K, Yamada Y, Taniguchi H, Andrews P, Baer T, Ezell M, Halloy C, John D, Loftis B, Mohr R, Wong K. 2013. Revolutionizing climate modeling with Project Athena: A multi-institutional, international collaboration. *Bull. Am. Meteorol. Soc.* **94**: 231–245.
- Magaldi MG, Haine TWN. 2015. Hydrostatic and non-hydrostatic simulations of dense waters cascading off a shelf: the east Greenland case. *Deep-Sea Res. Part I-Oceanogr. Res. Pap.* **96**: 89–104.
- Manley G. 1938. Meteorological observations of the British East Greenland expedition, 1935–36, at Kangerdlugssuak, 68° 10' N, 31° 44' W. *Q. J. R. Meteorol. Soc.* **64**: 253–276.
- Moore GWK. 2003. Gale force winds over the Irminger Sea to the east of Cape Farewell, Greenland. *Geophys. Res. Lett.* **30**: 1894, doi: 10.1029/2003GL018012.
- Moore GWK. 2012. A new look at Greenland flow distortion and its impact on barrier flow, tip jets and coastal oceanography. *Geophys. Res. Lett.* **39**: L22806, doi: 10.1029/2012GL054017.
- Moore GWK, Renfrew IA. 2005. Tip jets and barrier winds: a QuikSCAT climatology of high wind speed events around Greenland. *J. Clim.* **18**: 3713–3725.
- Moore GWK, Pickart RS, Renfrew IA. 2011. Complexities in the climate of the subpolar North Atlantic: A case study from the winter of 2007. *Q. J. R. Meteorol. Soc.* **137**: 757–767.
- Moore GWK, Renfrew IA, Harden BE, Mernild SH. 2015. The impact of resolution on the representation of southeast Greenland barrier winds and katabatic flows. *Geophys. Res. Lett.* **42**: 3011–3018, doi: 10.1002/2015GL063550.
- Oltmanns M, Straneo F, Moore GWK, Mernild SH. 2014. Strong downslope wind events in Ammassalik, southeast Greenland. *J. Clim.* **27**: 977–993.
- Oltmanns M, Straneo F, Seo H, Moore GWK. 2015. The role of wave dynamics and small-scale topography for downslope wind events in southeast Greenland. *J. Atmos. Sci.* **72**: 2786–2805.
- Outten SD, Renfrew IA, Petersen GN. 2009. An easterly tip jet off Cape Farewell, Greenland. II: Simulations and dynamics. *Q. J. R. Meteorol. Soc.* **135**: 1934–1949.
- Petersen GN, Renfrew IA. 2009. Aircraft-based observations of air-sea fluxes over Denmark Strait and the Irminger Sea during high wind speed conditions. *Q. J. R. Meteorol. Soc.* **135**: 2030–2045.
- Petersen GN, Renfrew IA, Moore GWK. 2009. An overview of barrier winds off southeastern Greenland during the Greenland Flow Distortion experiment. *Q. J. R. Meteorol. Soc.* **135**: 1950–1967.
- Pickart RS, Spall MA, Ribergaard MH, Moore GWK, Milliff RF. 2003. Deep convection in the Irminger Sea forced by the Greenland tip jet. *Nature* **424**: 152–156.
- Rasmussen L. 1989. Greenland winds and satellite imagery. *Vejret, Dan. Meteorol. Soc.*, 32–37.
- Renfrew IA, Petersen GN, Outten S, Sproson D, Moore GWK, Hay C, Ohigashi T, Zhang S, Kristjánsson JE, Førø I, Ólafsson H, Gray SL, Irvine EA, Bovis K, Brown PRA, Swinbank R, Haine T, Lawrence A, Pickart RS, Shapiro M, Woolley A. 2008. The Greenland flow distortion experiment. *Bull. Am. Meteorol. Soc.* **89**: 1307–1324.
- Renfrew IA, Outten SD, Moore GWK. 2009a. An easterly tip jet off Cape Farewell, Greenland. I: Aircraft observations. *Q. J. R. Meteorol. Soc.* **135**: 1919–1933.
- Renfrew IA, Petersen GN, Sproson DAJ, Moore GWK, Adiwidjaja H, Zhang S, North R. 2009b. A comparison of aircraft-based surface-layer observations over Denmark Strait and the Irminger Sea with meteorological analyses and QuikSCAT winds. *Q. J. R. Meteorol. Soc.* **135**: 2046–2066.
- Sabine CL, Feely RA, Gruber N, Key RM, Lee K, Bullister JL, Wanninkhof R, Wong CS, Wallace DWR, Tilbrook B, Millero FJ, Peng T-H, Kozyr A, Ono T, Rios AF. 2004. The oceanic sink for anthropogenic CO<sub>2</sub>. *Science* **305**: 367–371.
- Saha S, Moorthi S, Pan H-L, Wu XR, Wang JD, Nadiga S, Tripp P, Kistler R, Woollen J, Behringer D, Liu HX, Stokes D, Grumbine R, Gayno G, Wang J, Hou Y-T, Chuang H-Y, Juang H-MH, Selig J, Iredell M, Treadon R, Kleist D, Van Delst P, Keyser D, Derber J, Ek M, Meng J, Wei HL, Yang RQ, Lord S, Van Den Dool H, Kumar A, Wang WQ, Long C, Chelliah M, Xue Y, Huang BY, Schemm J-K, Ebisuzaki W, Lin R, Xie PP, Chen MY, Zhou ST, Higgins W, Zou C-Z, Liu QH, Chen Y, Han Y, Cucurull L, Reynolds RW, Rutledge G, Goldberg M. 2010. The NCEP climate forecast system reanalysis. *Bull. Am. Meteorol. Soc.* **91**: 1015–1057.
- Sampe T, Xie SP. 2007. Mapping high sea winds from space: A global climatology. *Bull. Am. Meteorol. Soc.* **88**: 1965–1978.
- Silva-Sánchez N, Schofield JE, Mighall TM, Martínez Cortizas A, Edwards KJ, Foster I. 2015. Climate changes, lead pollution and soil erosion in south Greenland over the past 700 years. *Quatern. Res.* **84**: 159–173.
- Skamarock WC. 2004. Evaluating mesoscale NWP models using kinetic energy spectra. *Mon. Weather Rev.* **132**: 3019–3032.
- Skamarock WC, Klemp JB, Dudhia J, Gill DO, Barker DM, Duda MG, Huang X-Y, Wang W, Powers JG. 2008. ‘A description of the Advanced Research WRF version 3.’ Technical Note NCAR/TN-475+STR. National Center for Atmospheric Research: Boulder, CO.
- Smith RB. 1982. Synoptic observations and theory of orographically disturbed wind and pressure. *J. Atmos. Sci.* **39**: 60–70.
- Straneo F, Cenedese C. 2015. The dynamics of Greenland's glacial fjords and their role in climate. *Ann. Rev. Mar. Sci.* **7**: 89–112.
- Straneo F, Heimbach P. 2013. North Atlantic warming and the retreat of Greenland's outlet glaciers. *Nature* **504**: 36–43.
- Våge K, Pickart RS, Moore GWK, Ribergaard MH. 2008. Winter mixed layer development in the central Irminger Sea: The effect of strong, intermittent wind events. *J. Phys. Oceanogr.* **38**: 541–565.